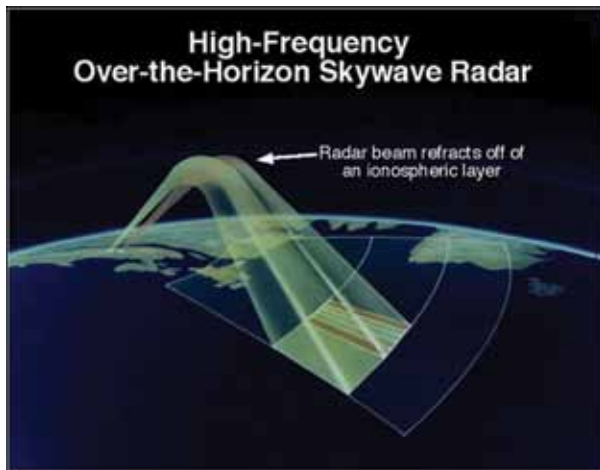


## High-Resolution Widesweep Backscatter Ionograms

G. San Antonio  
Radar Division

**Introduction:** High frequency (HF) over-the-horizon radar (OTHR) relies on the refraction of electromagnetic waves by the ionosphere to detect targets at very long ranges, typically more than 500 nmi (see Fig. 1). A fundamental aspect of successful target detection is the selection of an appropriate operating frequency to ensure a large amount of backscatter energy at the desired surveillance range. HF OTHR operates over four octaves of frequency (5 to 30 MHz) and highly variable (spatially and temporally) ionospheric conditions. For



**FIGURE 1**  
Illustration of HF OTHR ionospheric refractive propagation behavior.

these reasons, all modern HF OTHR systems use several techniques for real-time monitoring of ionospheric propagation conditions. The widesweep backscatter ionogram (WSBI) is an ionospheric sounding method in which backscatter energy is mapped as a function of range, azimuth, and frequency. This sounding method has been used for over 50 years in various systems.<sup>1,2</sup> Recently in 2011, the NRL Radar Division advanced the WSBI sounding method by producing high azimuthal resolution WSBI using the 2.5 km receive aperture of the Navy's AN/TPS-71 Relocatable OTHR (ROTHR) system. This represents a more than 5× increase in the azimuthal resolution over any previously produced WSBI sounding. Reference 3 provides further details concerning the history of WSBI sounding systems and the details of the current experimental configuration.

**High-Resolution WSBI:** High-resolution widesweep backscatter ionograms (HRWSBIs) have not been used in any previously fielded HF OTHR because

of constraints related to radar receiver hardware. The typical HF OTHR receiver is a single-channel narrowband device. In fact, the HRWSBIs that NRL has demonstrated could only be produced using an experimental reconfiguration of the ROTHR system. Current work under way in the area of Next Generation (Next-Gen) HF OTHR proposes the use of wideband direct digital receivers that can support multiple simultaneous digital downconversion channels, thus allowing simultaneous usage of a single receiver aperture for several purposes. The HRWSBI is just one possible function of a NextGen Common Receive Aperture architecture. The goal of the work described in this article was to investigate how the current-generation OTHR hardware can be used to investigate a potential NextGen capability and to understand what new information can be learned about the behavior of the ionosphere.

Using a very long baseline uniform filled array to produce HRWSBIs has several advantages over lower-resolution measurements:

1. increased azimuthal resolution
2. improved leading edge detection
3. finer ray-tracing for improved geolocation accuracy
4. increased understanding of ionospheric spatial-temporal variation
5. improved target detection via improved frequency selection advice
6. enhanced detection of ionospheric tilts (could cause out-of-plane propagation).

One of the main uses for WSBI measurements is for generating a three-dimensional electron density model of the ionosphere,  $u(x,y,z)$ . Once obtained, this model can be used in combination with geometric optics ray-tracing algorithms to compute coordinate registration maps linking radar space coordinates (range, azimuth) to ground coordinates (latitude, longitude). The process of converting the WSBI backscatter function  $s(r,\theta,f)$  to  $u(x,y,z)$  is a fundamentally ill-posed problem. A large amount of regularization is required under normal circumstances using low-resolution WSBI data,  $s_{\text{low}}(r,\theta,f)$ . HRWSBI data,  $s_{\text{high}}(r,\theta,f)$ , should decrease the amount of regularization required and produce estimates of the 3D electron density that are more faithful to the truth, ultimately yielding improved target geolocation. No quantitative results in this area have been produced so far; however, work is under way to incorporate HRWSBIs into current ionospheric modeling tools such as CREDO.<sup>4</sup>

**Results:** Several qualitative results have been derived from the experimental HRWSBI collection that was performed in 2011 using the ROTHR system. These results relate to the identification of small-scale

ionospheric phenomena. Figure 2 shows a two-dimensional slant-range vs azimuth slice through a three-dimensional (frequency, range, azimuth) HRWSBI. This piece of data displays the backscatter propagation at 23.01 MHz. The propagation is characterized by a “skip zone” in which no energy is refracted by the

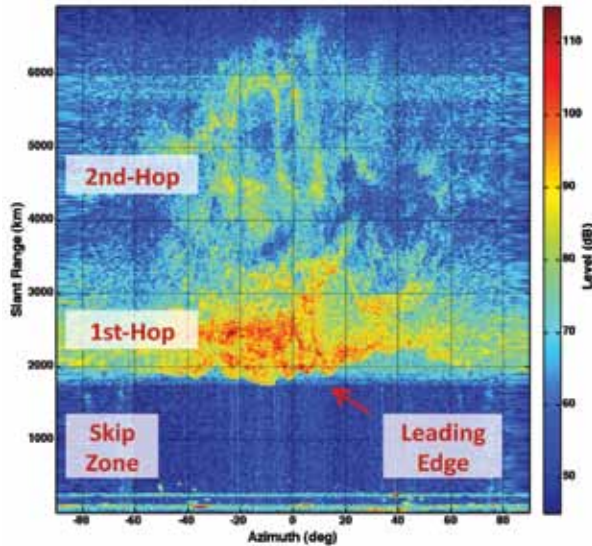


**FIGURE 2** High-resolution backscatter ionogram measurement. This backscatter ionogram was measured with an array having a 0.25° beamwidth, which reveals fine details in the ionosphere structure.

ionosphere due to the combination of a high elevation angle and high frequency. Backscatter energy begins to appear at what is called the “leading edge” around 2000 km slant range. Beyond the leading edge, there is a region of approximately 1000 km characterized by single-hop propagation followed by an extended region of double-hop propagation. The interesting feature that the HRWSBI reveals is the corrugated and highly structured behavior of the leading edge. This feature is caused by a nonsmooth underside ionosphere, which is indicative of a traveling ionospheric disturbance (TID). This is also indicated by the leading edge behavior shown in Fig. 3. Another feature that has been identified in the HRWSBIs is shown in Fig. 4. This figure shows a slant-range vs frequency slice for a single high-resolution beam steered to boresight. In this case, the backscatter energy is due to ionospherically refracted electromagnetic waves that backscatter from the surface of the ocean. One of the properties of HF ocean backscatter is that it is mainly composed of a vertical polarization component. When this property is combined with vertically polarized transmit and receive antennas and an ionosphere supporting two characteristic polarizations, the result is a range and frequency polarization “thumbprint” in a HRWSBI. This can be

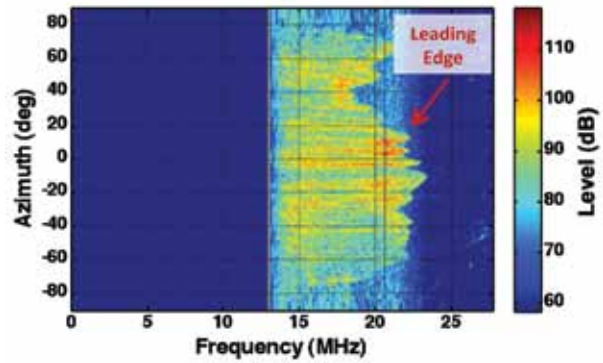


**FIGURE 3** Backscatter ionogram illustrating propagation behavior over frequency and azimuth for an isolated range cell. Leading edge variation indicates ionosphere spatial electron density variation.

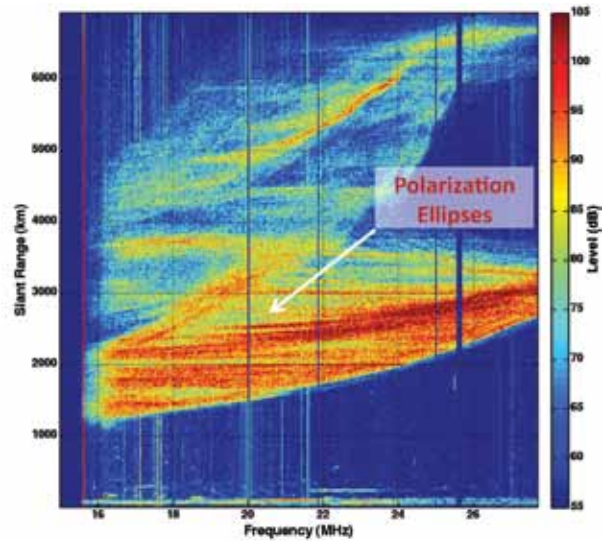


**FIGURE 4** Single high-resolution azimuth beam backscatter ionogram showing propagation polarization fading phenomena only visible using narrow beamwidth measurements.

seen as concentric ellipses of constant polarization in the WSBI.

**Summary:** This article describes recent experimental results obtained by the NRL Radar Division in producing high-resolution widesweep backscatter ionograms using the AN/TPS-71 ROTH system. Several small-scale ionospheric phenomena have been identified with this sounding method. Further work in the future is planned to quantify the performance gains achievable with respect to geolocation accuracy and optimal frequency selection. This work represents an enabling technology for NextGen OTHR.

[Sponsored by the NRL Base Program (CNR funded)]

## References

- <sup>1</sup>T.A. Croft, "Sky-Wave Backscatter: A Means for Observing Our Environment at Great Distances," *Revs. Geophysics and Space Physics* **10**(1), 73–155 (1972).
- <sup>2</sup>G.F. Earl and B.D. Ward, "The Frequency Management System of the Jindalee Over-the-Horizon Backscatter HF Radar," *Radio Science* **22**(2), 275–291 (1987).
- <sup>3</sup>G. San Antonio, "High Azimuthal Resolution Widesweep Backscatter Ionogram Measurements: Initial Results," NRL Tech Memo, 5320–003, Jan. 4, 2012.
- <sup>4</sup>S.V. Fridman, "Improved WSBI Inversion for ROTH," Final Technical Report, AFRL-SN-RS-TR-1998-27, Mar. 1998.

---

---

## Real-Time Electronic Attack (EA) Effectiveness Monitoring

S.L. Beun and J.J. Genova (NRL retiree)  
*Tactical Electronic Warfare Division*

**Introduction:** Managing the threat posed by anti-ship missiles (ASMs) is a crucial element of the U.S. Navy's operational objective to project power from both the sea and littoral areas. Rapid reaction ship defense capability against the barrage attack of modern ASMs requires the warfighter to properly allocate hard-kill and soft-kill resources. A high level of situational awareness will result in a proactive engagement that uses assets effectively and efficiently.

Situational awareness of the effectiveness of soft-kill or electronic attack (EA) requires the ability to measure the internal decision states of the ASM. Under an Office of Naval Research (ONR)-funded Discovery and Invention (D&I) program, building upon results from a prior investigation funded by the NRL Electromagnetic Warfare base research program, research was performed to design and fabricate a sensor capable of estimating the ASM's internal decision state during its terminal phase. This sensor has undergone an in-depth performance analysis and both chamber and field testing to verify its capability of real-time assessment.

**Background Results:** Various methods of real-time EA effectiveness monitoring have been proposed over the years. For example, accurate measures of ASM location were used to estimate the ASM-to-ship miss distance. However, modern ASMs typically perform fast maneuvers while approaching their targets to reduce the risk of being destroyed by hard-kill. These maneuvers make it impossible to project the ASM's flight path to its intended target. An alternate approach exploits the radio frequency (RF) transmissions in the ASM's beam. It was proposed that these RF transmissions could be used to measure the ASM's internal decision state during its terminal phase in real time by a spe-

cially designed electronic support (ES) sensor. Previous NRL-led research with the Electrosiences Laboratory at the Ohio State University confirmed these theoretical results and showed that the RF observable is viable under tactical situations.

**Sensor Design:** The sensor was designed to measure real-time EA effectiveness during the ASM's terminal phase for a modern low probability of intercept (LPI) ASM. To achieve this goal, we analyzed extensively the design performance and error budget of the sensor. The results of the analysis concluded that the design was ready to be fabricated. In addition, the sensor was designed to be a part of the electronic warfare command and control (EWC<sup>2</sup>) suite. Therefore, the sensor is not a stand-alone system and needs to receive direction cueing and pulse descriptor words from the ES systems, as depicted in Fig. 5.

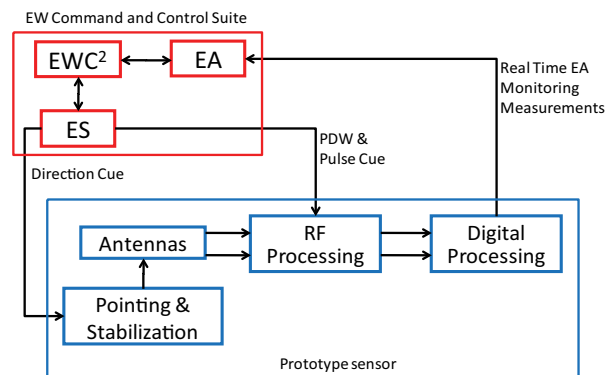


**FIGURE 5** Illustration of how the prototype sensor will fit within the EW command and control suite. The sensor will receive direction cueing and pulse descriptor words (PDW) from the ES sensors.

The sensor fabrication involved four components: antennas, RF processing, coherent digital processing, and real-time or post-processing analysis. Antenna alignment needed to account for antenna bias, ASM roll, monopulse noise, and ship pitch. The sensor needed the appropriate sensitivity to sense LPI signals. In order to exploit the ASM RF information, observable but weak signals need to be detected and properly processed.

The fabrication of the sensor focused on choosing the appropriate antennas and antenna control system to fit our design analysis for demonstration testing, and creating a coherent digital processing algorithm necessary to observe and reliably use these weak signals. The RF processing was customized for this sensor and included a wideband low noise amplifier system, dual matched tuners, and a local oscillator distribution with isolation. A prototype was fabricated in 2011 by NRL EW Support Measures Branch personnel. Figure 6

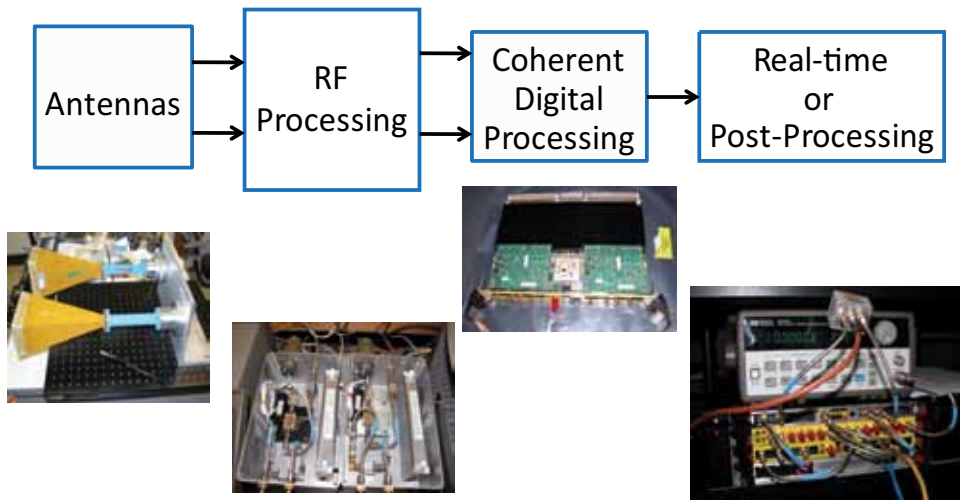


**FIGURE 6**  
Stand-alone prototype sensor.

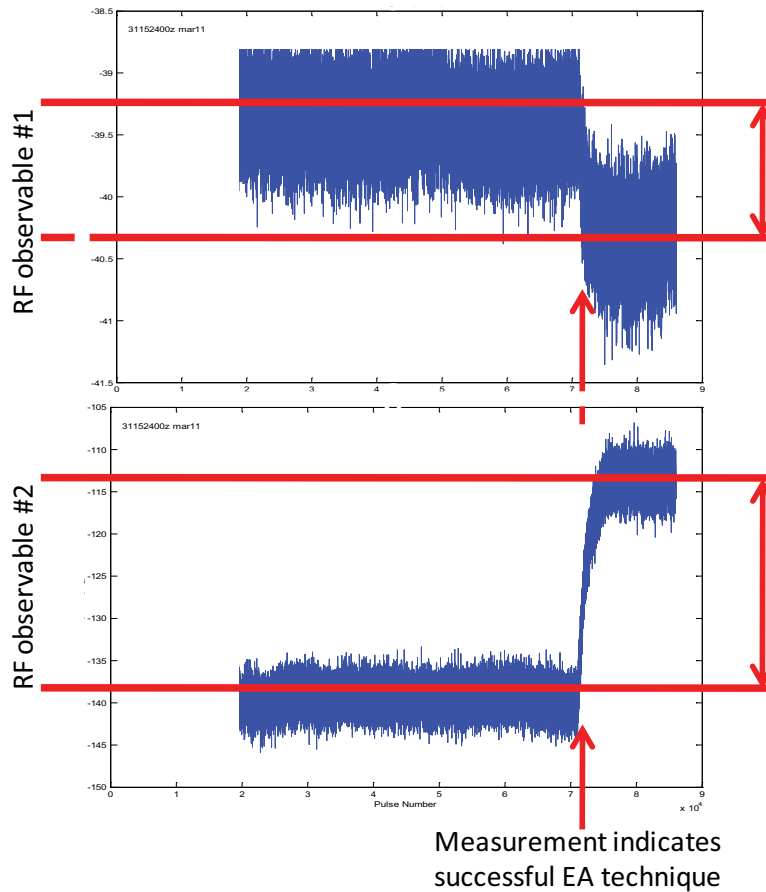


**FIGURE 7**  
Example of anechoic chamber test results. Horizontal axis is time during an engagement, and the vertical axis measures parts of the RF observable. The change in the measured observable indicates that the EA technique performed at that time was successful.

shows the general prototype sensor design and hardware.

**Test Results:** The prototype sensor fabricated by EW Support Measures Branch personnel has been used in both anechoic chamber testing and field testing. The anechoic chamber testing occurred in March 2011 in a chamber designed to test coordinated onboard and offboard countermeasures. The test involved the cooperation of the Surface EW Systems Branch's onboard Electronic Attack Test and Evaluation System (EATES) and the Offboard Countermeasures Branch's digital radio frequency memory (DRFM) offboard systems, along with the Integrated EW Simulation Branch's coherent radar-guided ASM simulators. Results confirmed previous research and many scenarios were performed to test the ES sensor feasibility. Figure 7 shows an example of the results.

Field testing was conducted at NRL's Chesapeake Bay Detachment (CBD) facility in August 2011. Static tests were conducted with the ASM simulator on the ground, and dynamic flight tests were conducted with the ASM simulator captive-carry on a Learjet. This testing involved coordination of assets and personnel stationed at CBD, on the water in the Chesapeake Bay, across the water on Tilghman Island, and on board the aircraft. Again, tests confirmed the capability of the ES sensor to monitor EA effectiveness in the tested scenarios.

**Summary:** Previous theoretical research and recent testing of the fabricated ES sensor show that real-time EA effectiveness monitoring is a viable tactical resource for the Navy. The end product of this research is a sensor that can produce real-time measurements of the ASM's decision state, providing a reliable element to situational awareness during an engagement.

[Sponsored by ONR]



---

---

## Diamond for Thermal Management in Power Electronics

T.J. Anderson,<sup>1</sup> M.J. Tadjer,<sup>2</sup> K.D. Hobart,<sup>1</sup> T.I. Feygelson,<sup>3</sup> J.D. Caldwell,<sup>1</sup> M.A. Mastro,<sup>1</sup> J.K. Hite,<sup>1</sup> C.R. Eddy, Jr.,<sup>1</sup> F.J. Kub,<sup>1</sup> and B.B. Pate<sup>1</sup>

<sup>1</sup> *Electronics Science and Technology Division*

<sup>2</sup> *Universidad Politécnic de Madrid, Spain*

<sup>3</sup> *SAIC, Inc.*

**Introduction:** As a wide bandgap semiconductor, gallium nitride (GaN) is attractive for next-generation power converters. The material demonstrates exceptional chemical and thermal stability, and it is capable

of handling high voltage and high current applications. Transistors based on this material system have a wide range of immediate Naval applications, such as high-power satellite communications and radar, unmanned underwater and aerial vehicles, ship drive components, and hybrid vehicle inverters. The capabilities of GaN-based circuits are limited by the self-heating effect, which generally refers to the resistive heating that occurs within the device under biased conditions, and results in degraded performance (such as current density and on-resistance). It is a significant problem for GaN-based electronics — the material is capable of high power density devices, thus the self-heating effect is more pronounced than in most other semiconductors. To mitigate self-heating, diamond has been proposed as a heat sink layer in the material structure, but efforts to date have resulted in poor device performance. Topside diamond approaches are known to degrade the device metallization, and efforts to grow the material structure on diamond substrates have resulted in increased defectivity or severe warping, neither of which is compatible with large-scale fabrication. The NRL Power Electronics Branch has developed the patented “gate after diamond” approach,<sup>1,2</sup> which enables the deposition of large-area diamond with minimal modifications to the process flow, and no adverse impact on device performance.

**NRL's Nanocrystalline Diamond:** The NRL diamond program is world renowned. Of particular interest to this work has been the development of the nanocrystalline diamond (NCD) process, in which a substrate is seeded in a suspension of nanocrystalline diamond powder, followed by diamond film growth in a hydrogen and methane atmosphere. The resulting films have a small grain size (~100 nm) and low roughness (5 nm rms), are optically transparent, and have a thermal conductivity three times higher than that of Cu (12 to 14 W/m-K).<sup>3</sup>

**Device Fabrication and Characterization:** The high electron mobility transistor (HEMT) was used as the test vehicle for this diamond work. The devices were fabricated at NRL using standard compound semiconductor fabrication steps, with the samples being split into two pieces — one to keep as a reference and one to be capped with the NCD layer. Self-heating is typically manifested as a negative slope in the saturation region of the  $V_{DS} - I_{DS}$  family of curves, shown in Fig. 8. The NCD-capped device demonstrates, in addition to a reduced negative slope, a lower on-resistance and comparable threshold voltage relative to the reference device.

**Channel Temperature Measurement:** The device operating temperature was initially characterized by

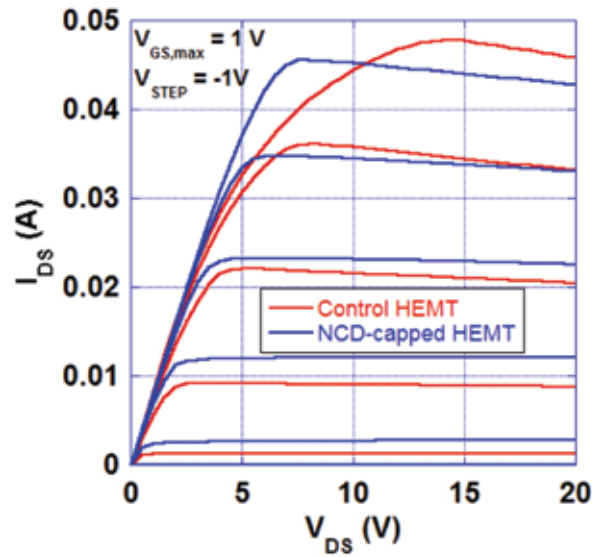


**FIGURE 8**  
Current–voltage characteristics for reference and NCD-capped HEMTs.

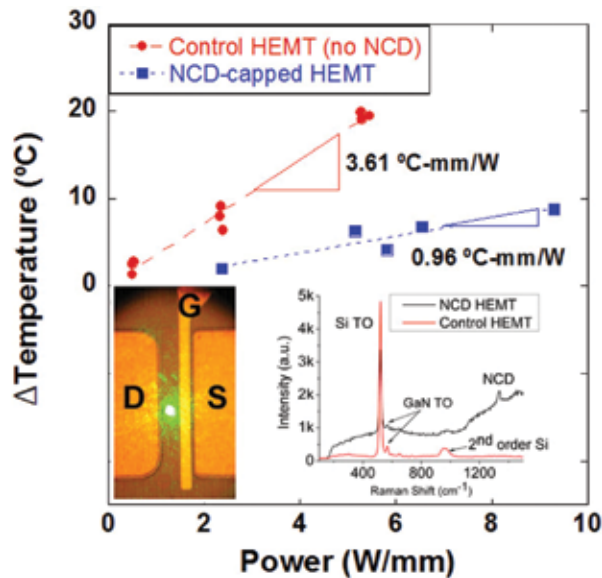


**FIGURE 9**  
Channel temperature as a function of DC power dissipation.

Raman thermography.<sup>4</sup> This measurement technique is based on the observation of a temperature-dependent shift in the characteristic Raman spectrum for GaN. The operating temperature of the transistor is calculated by observing the position of the GaN peak under biased conditions and referring to an experimentally determined calibration equation. As shown in Fig. 9, a linear correlation between DC power and channel temperature was demonstrated, and the NCD-capped device demonstrated a 20% lower operating temperature than that of the reference device. To validate this

measurement, IR imaging was performed on a biased device. Since GaN is transparent, one cannot directly image the active device layer without resorting to potentially destructive techniques such as painting the device black. One can, however, observe the temperature of the contact pads and draw some conclusions since they are very close to the channel. Figure 10 shows a reference and NCD-capped HEMT. It is apparent that the pads from the NCD-capped device are slightly hotter than those of the reference device. This observation supports the working theory that the diamond acts as a heat sink for the channel. Therefore, under biased conditions, more heat is dissipated from the channel to the contact pads, so one would expect the pads to be hotter but the channel to be cooler.

**Summary:** Reduced performance in GaN-based HEMTs as a result of self-heating has been well documented. Diamond has been proposed as an integrated heat sink layer, but the deposition conditions are harsh and sample size is limited, thus experiments have enjoyed limited success. The Electronics Science and Technology Division’s Power Electronics Branch has developed a “gate after diamond” approach using nanocrystalline diamond. Raman thermography was used to probe the channel temperature, and it was determined that NCD-capped devices had a 20% lower channel temperature at equivalent power dissipation. Electrical measurements indicate that NCD-capped devices have a higher current density, and lower on-resistance relative to a reference device, which leads to improved reliability and circuit efficiency. This is the world’s best diamond-capped device at the time of publication.

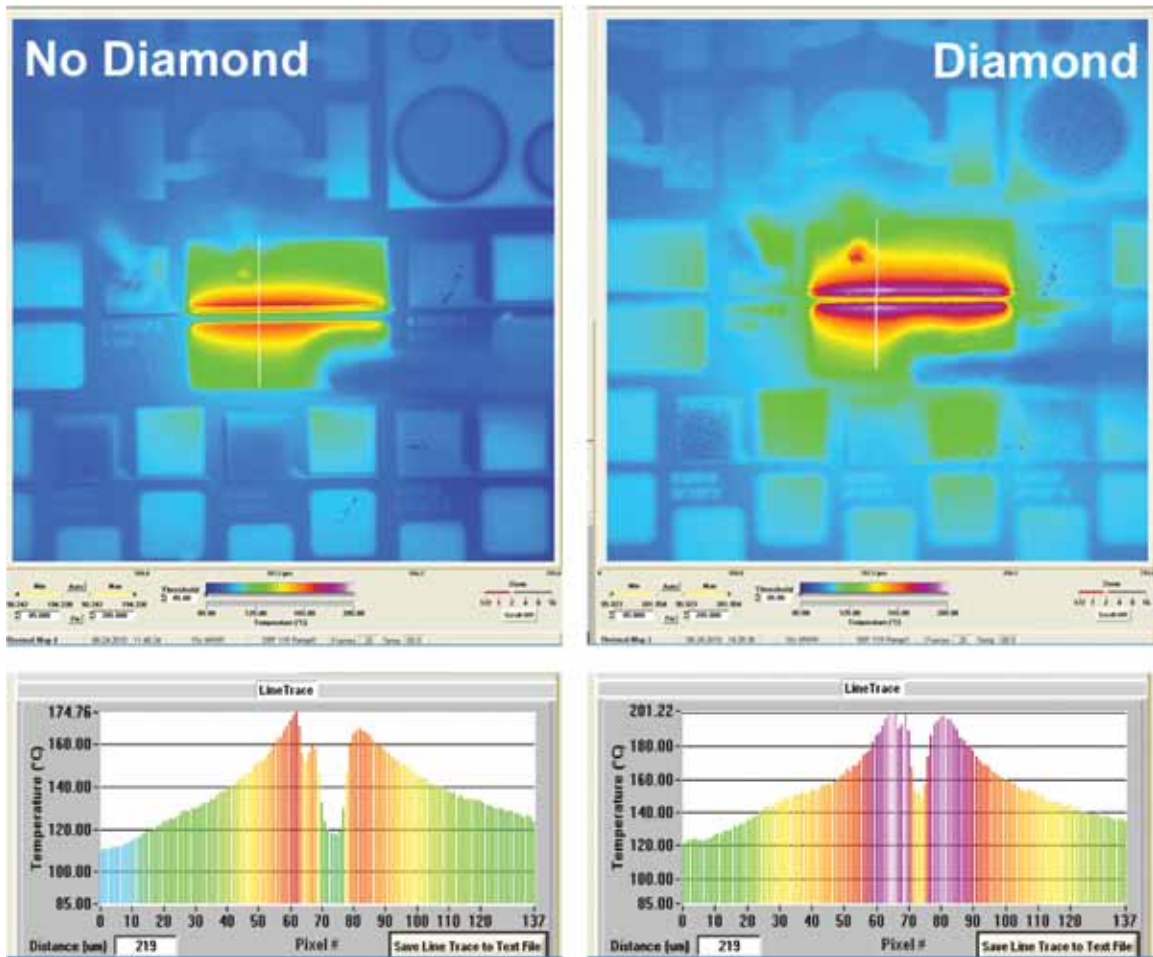


**FIGURE 10**  
IR images of reference (left) and NCD-capped (right) HEMTs under bias.

**Acknowledgments:** The authors are sincerely grateful to the microwave HEMT device group at NRL (S. Binari et al.) for insightful discussions and equipment use and to the NRL Institute for Nanoscience for equipment use and support. Material was provided by Nitronex Corporation. IR images were taken at the Air Force Research Laboratory (G. Via, E. Heller).

[Sponsored by the NRL Base Program (CNR funded)]

#### References

- <sup>1</sup> F. Kub and K. Hobart, "Gate After Diamond Transistor," U.S. Patent 8,039,301, Oct. 18, 2011.
- <sup>2</sup> M.J. Tadjer, T.J. Anderson, K.D. Hobart, T.I. Feygelson, J.D. Caldwell, C.R. Eddy, Jr., F.J. Kub, J.E. Butler, B. Pate, and J. Melngailis, "Reduced Self-Heating in AlGaIn/GaN HEMTs Using Nanocrystalline Diamond Heat-Spreading Films." *IEEE Electr. Dev. Lett.* **33**(1), 23–25 (2012).
- <sup>3</sup> J.E. Butler and A.V. Sumant, "The CVD of Nanodiamond Materials," *Chem. Vapor Deposition* **14**(7/8), 145–160 (2008).
- <sup>4</sup> J.B. Cui, J. Ristein, and L. Ley, "The Electron Affinity of the Bare and Hydrogen Covered Single Crystal Diamond (111) Surface," *Phys. Rev. Lett.* **81**, 429–432 (1998).

